Thermal denaturation of a helicoidal DNA model

Maria Barbi*

Laboratoire de Physique Théorique des Liquides, Université Pierre et Marie Curie, 4 Place Jussieu, 75252 Paris Cedex 05, France

Stefano Lepri[†]

Istituto Nazionale per la Fisica della Materia, UdR Firenze, via G. Sansone 1, 50019 Sesto Fiorentino, Italy

Michel Peyrard[‡]

Laboratoire de Physique, École Normale Supérieure de Lyon, 46 Allée d'Italie, 69364 Lyon Cedex 07, France

Nikos Theodorakopoulos[§]

Theoretical and Physical Chemistry Institute, National Hellenic Research Foundation, Vasileos Constantinou 48, Athens 11635, Greece

We study the static and dynamical properties of DNA in the vicinity of its melting transition, i.e., the separation of the two strands upon heating. The investigation is based on a simple mechanical model which includes the helicoidal geometry of the molecule and allows an exact numerical evaluation of its thermodynamical properties. Dynamical simulations of long-enough molecular segments allow the study of the structure factors and of the properties of the denatured regions. Simulations of finite chains display the hallmarks of a first order transition for sufficiently long-ranged stacking forces although a study of the model's "universality class" strongly suggests the presence of an "underlying" continuous transition.

PACS number(s): 87.15.Aa, 05.20.−y

I. INTRODUCTION

The study of simple dynamical models describing various features of DNA dynamics has interested many authors for almost 20 years [1]. This vivid interest arises of course from the biological relevance of DNA but also from its physical properties which can now be probed through single-molecule micromanipulation experiments like stress-induced transitions [2] or strand separation [3]. This series of studies has clearly pointed out that DNA must be considered as a dynamical object, whose (nonlinear) distortions could play a major role in its functions.

One feature of DNA that attracted a lot of attention from physicists is its thermal denaturation, i.e., the transition from the native double-helix B-DNA to its melted form where the two strands spontaneously separate upon heating [4], because it provides an example of a *one-dimensional phase transition*. Experiments show that this transition is very sharp, which suggested that it could be first order and this led to numerous investigations, first to justify the existence of a transition in a one-dimensional system and second to determine its order [5–12]. In spite of these efforts the nature of the transition is still unclear and moreover, as discussed below, the determination of its "true" order from experiments may turn out to be virtually impossible.

In the theoretical approaches, the level of complexity is reduced to the minimum by taking into account only the (classical) motion of large subunits rather than the full (quan-

tum) many-body dynamics of all the atoms. Clearly, an appropriate choice of the relevant degrees of freedom, depending on the specific problem at hand, is crucial. Models based on the theory of polymers use self-avoiding walks to describe the two strands [10–12]. They can be very successful in studying the properties of the melting transition at the largest scale but, as they do not describe DNA at the level of the base pairs, they cannot be used to investigate properties that depend on the sequence, or probe DNA at a microscopic scale such as some recent single-molecule experiments. One of the simplest models that investigates DNA at the scale of a base pair is the Peyrard-Bishop (PB) model [13–15]. The complex double-stranded molecule is described by postulating some simple effective interaction among the bases within a pair and along the strands. The model has been successfully applied to analyze experiments on the melting of short DNA chains [16]. Furthermore, it allows to easily include the effect of heterogeneities [17] yielding a sharp staircase structure of the melting curve (number of open base pairs as a function of the temperature T) [4]. Beyond its original motivation to explain the denaturation transition, the PB model has an intrinsic theoretical interest as one of the simplest one-dimensional systems displaying a genuine phase transition [8,9].

The PB model has, however a serious shortcoming because it does not take into account the helicoidal structure of DNA. In the following, we consider an extended version of the PB model that has been proposed to avoid this weakness [18,19]. The introduction of DNA geometry induces an important coupling between base pair opening and helical twist, largely substantiated for real DNA [18]. A modified version of this helicoidal model has also been successfully applied to describe the denaturation of the chain induced either thermally or mechanically by applying an external torque to the

*Electronic address: barbi@lptl.jussieu.fr
[†]Electronic address: stefano.lepri@unifi.it
[‡]Electronic address: Michel.Peyrard@ens-lyon.fr
[§]Electronic address: nth@eie.gr

68 061909-1

chain ends [20]. Furthermore, its nonlinear excitations have been studied: small amplitude breather-like solutions have been analytically determined [21] as well as large localized bubbles [22]. Both types of excitations are of interest as they may be thermally excited as precursors for the DNA strand separation. A first effect of the helicoidal structure, namely to bring close to each other bases which are not consecutive in the sequence, was treated in [23], by introducing an interaction between these bases. This first approach however did not take into account the important geometrical effect that we want to examine here, the coupling between opening and twist.

The aim of this work is to give further insight on the melting transition of the helicoidal model, both from the statistical and from the dynamical point of view. After having recalled the model and its state variables (Secs. II and III), the first part (Secs. IV and V) is devoted to its exact thermodynamics and to a simulation study of its statistical properties. We find that the melting transition is extremely sharp, bearing essentially all of the hallmarks of a first-order transition, at all temperature sampling steps studied (down to 0.01 K). However, a study of the model's "universality class," using finite-size scaling techniques, allowing some variation of the relevant physical parameters, and drawing from analogies with a Schrödinger-like equation (the Appendix), strongly suggests the presence of an "underlying" continuous transition of the Kosterlitz-Thouless type in the absence of nonlinear stacking. This should be contrasted with the exact second-order transition obtained in the zero-stacking limit of the PB model [9].

In the second part (Sec. VI) we investigate dynamical structure factors that are of particular relevance to both neutron [24] and Raman [25] scattering experiments. The underlying idea is that, upon approaching the transition, the molecule should display precursor effects in the form of a "mode softening," i.e., a slowing-down of the dynamics with appearance of a low-frequency component in the spectrum. Slowing effects have been, to some extent, observed in the structure factors of the PB model [15] thus encouraging this type of investigation.

II. THE HELICOIDAL MODEL

Two versions of the model have been proposed in earlier studies. The first one [18] describes an elastic backbone and fixed base-pair planes while the second [20] considers a rigid backbone and moving base-pair planes. The two models display a very similar behavior with respect to denaturation as the potentials associated to the base-base interactions in a pair and along the strands are the same in both cases, and because both introduce a coupling between opening and twist that results from the helicoidal geometry. In the following, we will consider the fixed-planes model, sketched in Fig. 1.

The helical structure of DNA is introduced essentially by the competition between a stacking interaction that tends to keep the base-pairs close to each other (given by the fixed distance h between the base planes) and the length $\ell_0 > h$ of the backbone segment (described as an elastic rod of rest
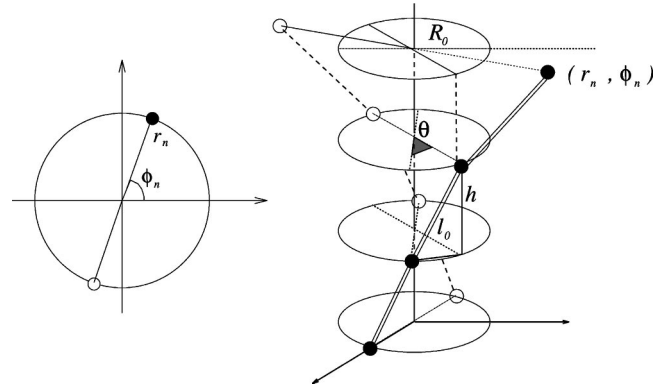

FIG. 1. Schematic representation of the fixed-planes DNA helicoidal model.

length ℓ_0) that connects the attachment points of the bases along each strand. The ratio ℓ_0/h fixes the strand slant and therefore the resulting helicity of the structure. This helicity is accounted for by the angle of rotation of a base-pair with respect to the previous one, namely the *equilibrium twist angle* θ, equal to $2\pi/10.4$ in B-DNA at room temperature.

In the model, bases are described as pointlike particles of equal masses m joined by elastic rods along each strand. Bases lying on the same plane are coupled by hydrogen bonds leading to an attractive force that tends to maintain their equilibrium distance equal to the DNA diameter $2R_0$. We assume that the two bases in each pair move symmetrically. To describe base-pair opening and helical torsion under those constraints, it suffices to introduce two degrees of freedom per base-pair: these are r_n and ϕ_n, i.e., the radial and angular positions and of the nth base. The total number of degrees of freedom is thus $2N$, N being the total number of base pairs. The restriction imposed by the assumption of a symmetric motion preserves the essential feature of the helical structure, the coupling between torsion and opening, while it keeps the model sufficiently simple to allow an *exact* treatment of its thermodynamics.

We consider the Lagrangian [26]

$$\mathcal{L} = m\sum_n (\dot{r}_n^2 + r_n^2\dot{\phi}_n^2) - D\sum_n (\exp[-a(r_n - R_0)] - 1)^2$$

$$- K\sum_n (l_{n,n-1} - \ell_0)^2 - S\sum_n (r_n - r_{n-1})^2$$

$$\times \exp[-b(r_n + r_{n-1} - 2R_0)], \tag{1}$$

where $\ell_0 = \sqrt{h^2 + 4R_0^2\sin^2(\theta/2)}$ and $l_{n,n-1}$ are respectively the equilibrium and the actual distance between the two bases n and $n-1$ along a strand,

$$l_{n,n-1} = \sqrt{h^2 + r_{n-1}^2 + r_n^2 - 2r_{n-1}r_n\cos(\phi_n - \phi_{n-1})}. \tag{2}$$

For later purposes, it is convenient to introduce the local twist angle defined as $\theta_n = \phi_n - \phi_{n-1}$.

The first term in the Lagrangian is the kinetic energy. The second term is intended to describe the hydrogen bond interaction between the two bases in a pair. Following Refs. [13]

TABLE I. The parameter set used throughout the paper.

Parameter	Symbol	Value	
Morse potential range	a	6.3	Å^{-1}
Stacking interaction range	b	0.5	Å^{-1}
Morse potential depth	D	0.15	eV
Stacking interaction coupling	S	0.65	eV Å^{-2}
Interplane distance	h	3.4	Å
Elastic coupling	K	0.04	eV Å^{-2}
Equilibrium distance	R_0	10	Å
Twist angle	θ	0.60707	rad
Base masses	m	300	amu

FIG. 2. A sketch of the behavior of first-order transition curves in the three planes defined by the DNA model parameters $-\sigma$, Γ, and T. Γ_D and T_D represent the transition torque and temperature, respectively; (a) thermally-induced denaturation "isobar" at zero torque; (b) coexistence curve; (c) torque-induced denaturation isotherm at $T=T_D$, corresponding to a zero critical torque.

and [18], a simple Morse potential form is chosen. The quadratic term in $(l_{n,n-1} - \ell_0)^2$ represents the elastic energy of the backbone rods between neighboring base-pairs on each strand. Finally, the last term models a stacking interaction between neighboring base pairs. Its effect is to decrease the stiffness of the open parts of the chain relatively to the closed ones and to stabilize the latter with respect to the denaturation of a single base-pair. Terms of this type increase the cooperative effects close to the melting transition [15,27].

In the present paper we restrict our attention to a chain with free boundary conditions, which corresponds to the experimental situation when DNA denaturation is studied in solution. However, the model described above can be easily modified to account for an external torque Γ applied at the base pairs at the two ends [20], as it is done in some single-molecule experiments.

The geometrical parameters of the model can be straightforwardly fixed according to the available structural data [18]. Much more delicate is instead the choice of the parameters b, D, S and K gauging the effective forces. We selected values similar to those previously considered for the fixed-planes case, which have been discussed elsewhere: the choice of the K parameter can be independently derived [27] from the twist persistence length [28], while the choice of the other two parameters was based [29] on a comparison with recent mechanical denaturation experiments [2]. In particular, the important parameter D which sets the main energy scale, has been tuned to reproduce as closely as possible the experimental value of the denaturation temperature $T_D = 350$ K. The full set of parameters used in the following are summarized in Table I.

For the numerics it is convenient to work in dimensionless units. A suitable choice is to measure lengths and energies in the natural units of the Morse potential, a^{-1} and D, respectively, whereby time is expressed in units of $\sqrt{m/Da^2}$. With the parameters of Table I, one time unit (t.u.) $\simeq 2.3$ ps.

III. THE DENATURATION TRANSITION: A QUALITATIVE DISCUSSION

Before going on, it is instructive to briefly discuss the thermodynamic state variables of the chain as well as the (possible) analogies between denaturation and the more familiar liquid-gas transition.
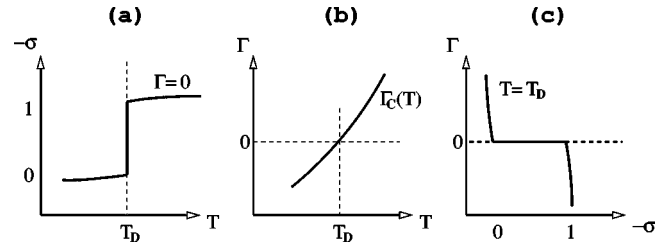
As already pointed out [20], the applied torque Γ plays the role of the pressure P for the liquid-gas system. Its conjugate variable is the *degree of supercoiling* σ. Since we do not consider the curvature of the axis of the helix, it reduces simply to the *average twist*:

$$\sigma = \sum_n^N \frac{(\langle \theta_n \rangle - \theta)}{N\theta}. \qquad (3)$$

This variable thus plays the role of the volume V. Following this analogy we can therefore establish the following correspondences:

DNA model		liquid-gas
T	$\leftrightarrow$	T
Γ	$\leftrightarrow$	P
$-\sigma$	$\leftrightarrow$	V

The sign of σ is chosen for convenience as the degree of supercoiling vanishes for B-DNA and is negative for a partially denatured chain [see also Eq. (4) below].

Two natural scenarios may thus be expected: an isothermal, torque-induced denaturation at $\Gamma = \Gamma_D$ or a fixed-torque, thermally-induced one at $T = T_D$. For the liquid-gas case, these two situations correspond to crossing of the coexistence curve in the (P,T) plane with an horizontal or a vertical line, leading to the transitions classically described by isotherms in the (P,V) plane or by isobars in the (V,T) one, respectively. In both cases, the presence of a constant-temperature or a constant-pressure/torque domain is associated to the phase coexistence.

Within this analogy, the transition isotherms correspond to the curves in Fig. 3 of Ref. [20], and reproduced schematically, on the $(\Gamma, -\sigma)$ plane, in Fig. 2(c). Conversely, the thermal denaturation at constant torque $\Gamma = 0$ are correctly described in the $(-\sigma, T)$ plane [Fig. 2(a)]. Notice that, with the convention that a negative Γ corresponds to an untwisting torque, both Γ_D and T_D must increase upon increasing temperature and torque respectively [see Fig. 2(b)]. However the negative torque cannot exceed some critical value without leading to an instability of the helix associated to a change of the sign of the helicity. In the following, we will focus on the thermal denaturation transition at $\Gamma = 0$.

It is important to remark that the helical constraints included in the model roughly impose, at vanishing external torque, $\theta_n \approx \theta$ for a closed chain segment, and $\theta_n \approx 0$ for the denatured one. This follows from the geometry of the helix and the stiffness of the strands: since the distance between consecutive bases is constrained by the elastic rods to be approximately equal to ℓ_0, θ_n is of order ℓ_0 / r_n and hence very small for $r_n \gg R_0$. Let us denote by n_d the average number of open bases in a chain of length N. Provided that open and closed regions coexist along the helix, and that they are spatially well separated (this is well confirmed by simulations as we show below), then, to a good approximation, we have

$$-\sigma \approx -\frac{n_d(-\theta)}{N\theta} = \frac{n_d}{N}. \tag{4}$$

The latter quantity in nothing but the average fraction of open base pairs $\rho = n_d / N$ and the "isobar" $-\sigma(T)$ can thus be identified with the familiar denaturation curve $\rho(T)$. In other words, the supercoiling and the fraction of open base pairs are equivalent order parameters.

Before going further there is one crucial issue that should be addressed. One may argue that for a one-dimensional model like the one at hand no phase transition of any type should be observed. However, all usual arguments against the existence of singularities in thermodynamic potentials have been showed *not to hold* for the PB model [9]. Since the latter is in many respects similar to the helicoidal model, the same arguments apply and a genuine phase transition is not forbidden *a priori*. This is confirmed by the transfer integral approach which can be carried exactly (although partly numerically) for this simple model.

IV. TRANSFER INTEGRAL APPROACH

A. "Apparent" thermodynamics

Because the model is one dimensional, a direct calculation of the partition function can be performed by the transfer integral (TI) method, as it was done for the simpler PB model [15]. The calculation proceeds along the same lines, but it is more involved because the model has two degrees of freedom (r_n and ϕ_n) per unit cell. It nevertheless reduces to a one-dimensional TI equation because the contribution introduced by the angular part can be diagonalized by a Fourier transform [20,29]. As the calculation has already been presented in these earlier studies we do not discuss the method here and we confine our attention on its results, which point out new aspects of the transition that had been overlooked.

In this subsection we restrict ourselves to results obtained via numerical solution of the TI equation. The accuracy of this approach is limited first by discretization errors in the integrations and by the need to numerically evaluate integrals over an infinite domain. As discussed in the next subsection, this second restriction can be partially lifted by a finite size scaling analysis, which involves a properly controlled approach to infinity. Integration methods, such as the Gauss-Legendre quadrature which select appropriate absissa

for the evaluation of the function according to the number of points involved in the calculation, are also useful to integrate over a large domain with a reasonable number of points. For this first study, in order to ensure that all integrals are evaluated with the same discretization error, we have computed them with a 10th order Bode's method [30] with a fixed spatial step $\delta r = 0.032$ Å and a minimum value $r_{min} = 9.7$ Å (due to the strong repulsion between bases described by the Morse potential, r cannot take values significantly below the equilibrium length of 10 Å). The maximum r_{max} of the integration range depends on the number of integration points, which has been varied from 631 to 3601 leading to $29.9 \leq r_{max} \leq 124.9$ Å. The eigenvalues of the transfer integral operator have been obtained either by diagonalization of the equivalent matrix problem or by the Kellog's method [31] to get the two lowest eigenvalues.

The eigenvalues Λ of the TI operator will henceforth be written as $\Lambda = \exp(-\epsilon/k_B T)$ where k_B is the Boltzmann constant. With this notation the free energy per particle is determined by the smallest ϵ eigenvalue ϵ_0 and is given by

$$f = -k_B T \ln(4\pi m k_B T) + \epsilon_0. \tag{5}$$

Relevant thermodynamic quantities like the entropy and specific heat are then evaluated from the standard relations

$$s = -\frac{\partial f}{\partial T}, \quad c_v = -T\frac{\partial^2 f}{\partial T^2}. \tag{6}$$

The mean base-pair stretching is given by

$$\langle r \rangle = \int_0^{+\infty} r |\phi_0(r)|^2 dr, \tag{7}$$

where ϕ_0 is the eigenfunction associated with ϵ_0.

The free energy f and the mean value of the base pair stretching $\langle r \rangle$ for our model are shown in Fig. 3, for temperatures going from 349 to 352 K with a step of 0.02 K. Within the accuracy of the calculation, a cusp in f at $T_D = 350.74$ K is distinctly seen. It is associated with a sharp jump of the entropy at the transition. A jump in the specific heat is also observed. Evaluating numerically the first and second left and right derivatives of the free energy, one obtains the jump in entropy $\Delta s = 4.40\, k_B$, or 8.75 cal/K/mol, and the jump in specific heat $\Delta c_v = 0.64\, k_B$. The specific heat drops from 2.14 k_B below T_D to $c_v = 1.5\, k_B$ for $T > T_D$ as expected from equipartition because after denaturation only the harmonic contributions of the hamiltonian stay significant.

Figure 3(b) shows that, within numerical accuracy, $\langle r \rangle$ exhibits a discontinuous transition from a finite constant value (very close to the equilibrium value R_0) to a value of the order of the system size; in other words, the eigenfunction ϕ_0 appears to become suddenly delocalized. The picture of a sharp transition persists down to a temperature sampling of 0.01 K.

Although the numerical results strongly suggest the occurrence of a first order transition, caution is necessary: previous studies of the related PB model have shown that the nonlin-
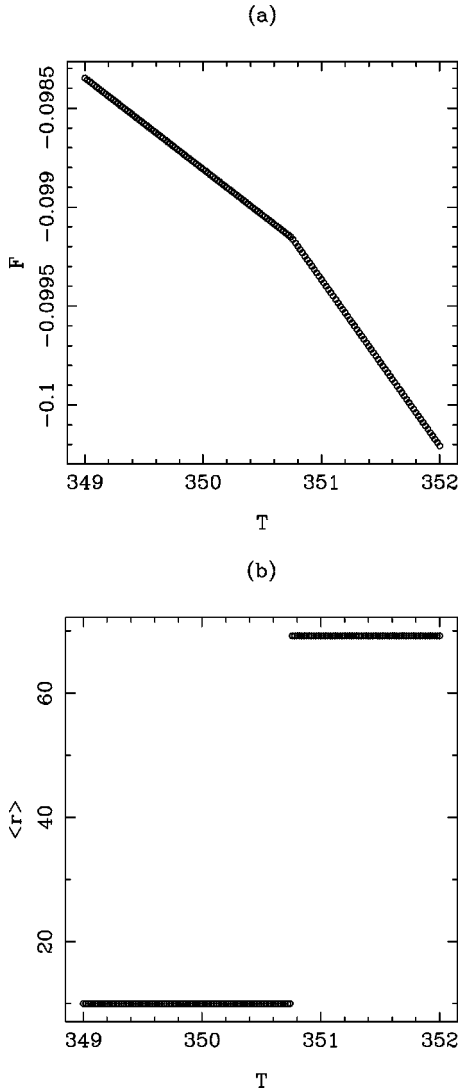
FIG. 3. The free energy per particle f (a), and the mean value of the base pair stretching $\langle r \rangle$ (b) of the model evaluated by the transfer integral method in the temperature range $349 \leqslant T \leqslant 352$ K with a step $\Delta T = 0.02$ K. The model parameters are those listed in Table I (calculation with the Bode's method, $\delta r = 0.032$ Å, $r_{min} = 9.7$ Å, and $r_{max} = 124.9$ Å).

ear stacking produces an extremely sharp, first-order-like behavior which masks the underlying second-order transition as long as one stays out of a very narrow domain in the immediate vicinity of the critical temperature T_D (exponential crossover [32,33]). A more complete picture of the properties of the transition will therefore be given in what follows.

B. The "underlying" transition

We first address the question of what happens in the absence of the nonlinear stacking, i.e., at $S = 0$. Preliminary numerical investigations suggest a smooth behavior, both of the lowest eigenvalue ϵ_0 and of the next-to-lowest, ϵ_1, as functions of temperature; an "avoided crossing" between them appears, with a small, but finite gap which has a mini-

mum at a certain temperature. Before we proceed to analyze the data obtained in detail, it is necessary to provide some background and notation.

The order of the phase transition of the ideal system of unconstrained transverse spatial extent is determined by the critical exponent ν which characterizes the gap $\Delta \epsilon \equiv \epsilon_1 - \epsilon_0 \propto (T_D - T)^{\nu}$ at temperatures below T_D; a value $\nu = 1$ implies a cusp in the free energy and a discontinuous entropy; a value equal to 2 implies a discontinuity in the specific heat, i.e., a usual 2nd order transition, etc.

The "raw" data provided by numerical solution of the TI equation refer to a particular transverse system size $L = r_{max}$ determined by the imposition of an upper cutoff to the integration. On the other hand, near a critical point of the infinite system, the transverse fluctuations of the order parameter also diverge. The quantity $\xi_{\perp} = \sqrt{\langle r^2 \rangle - \langle r \rangle^2}$ provides a measure of the distance from the critical point with dimensions of length. According to the finite-size scaling hypothesis [34], size-dependent properties of a system in the vicinity of the transition should depend solely on the ratio $L/\xi_{\perp}$, i.e.,

$$\Delta \epsilon_L(T) = L^{-\sigma} f_g \left(\frac{L}{\xi_{\perp}} \right), \tag{8}$$

where the exponent σ characterizes the rounding of the gap (cf. below), $f_g(0)$ is a nonzero constant, and $f_g(x) \propto x^{\sigma}$ as $x \gg 1$ guarantees size independence in the limit $L \to \infty$. In the simplest cases, the positions of the minima of the gap are related to the type of divergence of $\xi_{\perp}$; according to the above scaling scenario, the temperature $T_m(L)$ where the gap minimum occurs, is such that

$$\xi_{\perp}(T_D - T_m(L)) \approx L. \tag{9}$$

We have numerically solved the TI equation for a wide range of system sizes, using Gauss-Legendre quadratures, where L is defined as the largest grid point value provided by the Gauss-Legendre algorithm for the number N of grid points chosen for the calculation. Again, in order to ensure uniform accuracy, N grows proportionately to the system size, with $r_{max} = 350$ Å corresponding to $N = 2048$ points. Figure 4 shows the dependence of the minimal gap $\Delta \epsilon_L(T_m)$, and the corresponding temperature T_m on L. The gap appears to depend quadratically on $1/L$ [i.e., $\sigma = 2$ in Eq. (8)], to very good accuracy, with an estimated limit of 1.4×10^{-5} (with a standard deviation 0.8×10^{-5}) as $L \to \infty$. We note in passing that the disappearance of the gap between the bound state eigenvalue and the one belonging to the bottom of the continuum band provides numerical evidence for the true occurrence of an exact, thermodynamic phase transition [35]. The temperatures which correspond to the gap minima can be well fitted to the function

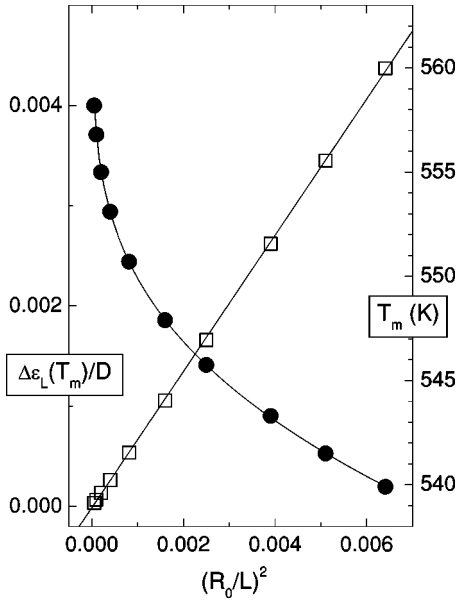$$T_m(L) = T_D \left[1 - \frac{a_2}{\ln\left(\dfrac{L}{R_0 c} \right)} \right] \tag{10}$$

FIG. 4. Dependence of the minimal difference between the lowest eigenvalues of the transfer integral operator $\Delta\epsilon_L(T_m)$ (open squares, left y axis) and temperatures T_m (closed circles, right y axis) versus $1/L^2$.

with $T_D = 577.8$ K, $a_2 = 0.170$ and $c = 0.94$. This type of dependence of T_m on L immediately suggests [cf. Eq. (9)] that

$$\xi_\perp = cR_0 e^{a_2/|\tau|}, \tag{11}$$

where $\tau = T/T_D - 1$.

Figure 5 shows that data taken from a wide range of system sizes scale well if plotted according to Eqs. (8) and (11). The numerical evidence thus strongly suggests that the underlying transition manifests itself as an essential singularity of the gap, of the Kosterlitz-Thouless (KT) type. Equations (11) and (8) then imply that, in the limit $L \to \infty$,

$$\Delta\epsilon \propto e^{-2a_2/|\tau|}. \tag{12}$$

In the Appendix, it will be possible to identify the origin of this particular behavior as an inverse-square attractive interaction between the stretching coordinates of successive base pairs.

C. Finite stacking revisited

It is now reasonable to conjecture, by analogy with what happens in the PB model, that the effects of the nonlinear stacking interaction will depend on its range. For the standard parameter set of Table I, the ratio $b/a = 0.079$ is very small indeed. What happens at a less extreme regime, $b/a = 0.190$, is shown in Fig. 6. Scaling according to the ansatz (11) holds within a fairly narrow range $|\tau| < 0.05$ around the denaturation point; note that it is the smaller magnitude of the nonuniversal parameter a_2 which is responsible for the narrowing of the asymptotic critical region. Figure 7 summarizes what happens at $b = 0.9$ Å^{-1}, i.e., $b/a = 0.143$, only slightly above the value of Table I. The gap exhibits an apparent critical exponent very close to unity down to τ
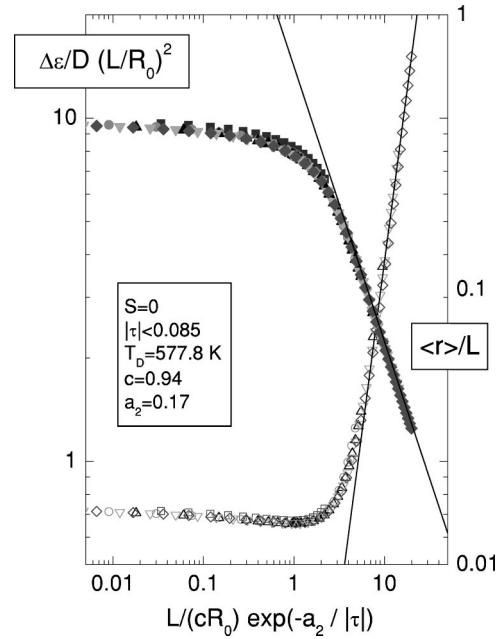

FIG. 5. Scaling of the difference between the two lowest eigenvalues of the transfer integral operator (open symbols, left y scale), and the order parameter (solid symbols, right y scale). The different points have been obtained by transfer integral calculations performed with 5 values of $L/R_0 = 16$, 35, 70, 100, and 140. The dotted lines have slopes 2 and -1, respectively, in accordance with the finite-size scaling hypothesis.
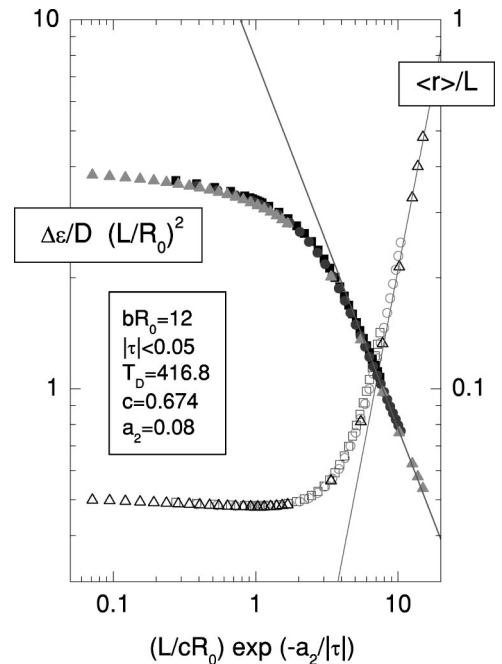

FIG. 6. Scaling of gap (open symbols, left y scale), and order parameter (solid symbols, right y scale); model parameters are those of Table I, with the exception of $b = 1.2$ Å^{-1}. The different points have been obtained by transfer integral calculations performed at $L/R_0 = 25$, 35, and 50. The dashed lines have slopes 2 and -1, respectively, in accordance with the finite-size scaling hypothesis.
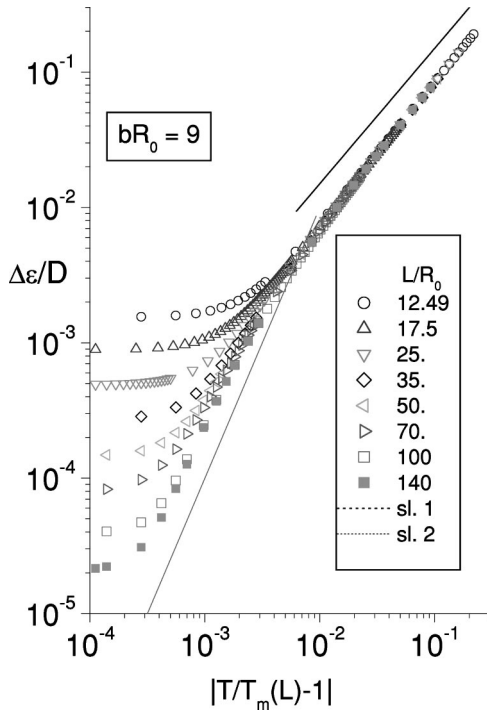
FIG. 7. Dependence of the gap on the reduced temperature $T/T_m - 1$ for $b = 0.9$ Å^{-1} and system sizes $L/R_0 = 12,49$, 17.5, 25, 35, 50, and 70. The dashed and dotted lines have slopes 1 and 2, respectively. Apparent first-order behavior prevails for $|\tau| > 0.01$; closer to the critical point there is a clear increase in the slope, before the onset of finite size rounding.

$= 0.01$; closer to the denaturation point, the effective slope increases significantly; it is reasonable to conjecture that at temperatures even closer to T_D, the asymptotic behavior will be dominated by the underlying essential singularity. At the physically relevant value of $b = 0.5$ Å^{-1}, crossover to the KT regime has moved below $\tau = 10^{-5}$ and is practically unobservable.

The analysis of this section demonstrates that, in spite of the very different mathematical properties of their "bare" versions, both the "straight" (PB) and the helicoidal DNA models, are effectively dominated by the stacking interaction when the latter is of sufficiently long range; because of it, for all practical purposes, the transition has all the characteristics of a first order transition, including a practically infinite discontinuity of the mean base pair stretching, and a latent heat. Similarly, at the transition temperature, a very small temperature gradient (of the order of the width of the transition region, i.e., $\Delta T < 0.001$ K) leads to an apparent phase coexistence and hence to many features that one would be tempted to qualify as "typical of a first-order transition" as shown in the next sections. These properties are very reminiscent of some results found on models of martensitic phase transitions [36–38], but because we are dealing with a one-dimensional model that has a genuine phase transition, the phenomenon is more remarkable here.

Our results provide an excellent example of the distinction between the "experimental" perspective and the "theoretical" one, regarding the definition of the order of a phase transition: although, in theory, the transition of the helicoidal DNA model is of infinite order (essential singularity), the actual temperature range over which it manifests its continuous character is far beyond the limits of either experimental or numerical observation.

V. MOLECULAR DYNAMICS

In this section we report the results of direct simulations of the model. They bring complementary information on the nature of the transition and allow us to study its dynamics as discussed in Sec. VI. As said above, we consider the case of thermal denaturation for $\Gamma = 0$ and free boundary conditions. Microcanonical and canonical simulations were performed because they allow the observation of the phase space from different viewpoints.

In the microcanonical ensemble, the Euler-Lagrange equations derived from Eq. (1) were integrated directly with the standard fourth-order Runge-Kutta method with a small enough time step (typically 0.02 t.u.) in order to insure that the relative energy drift is negligible (usually better than 10^{-5}) on the time scales of each run, i.e., 10^5 to 10^6 t.u. [39]. Initially, all particles are set in their equilibrium positions ($r_n = R_0$, $\phi_n = n\theta$) with random Gaussian distributed velocities (with zero average) in the radial direction. The variance of the distribution serves to fix the energy per degree of freedom e. The averaging of the quantities of interest is only started after a long enough transient to let the system equilibrate. After equilibration, the thermal energy $k_B T$ is computed in the usual way as twice the average kinetic energy per degree of freedom.

Constant-temperature (canonical) results were obtained through an extended Nosé-Hoover method using a thermostat chain [40] which is specifically designed to constrain the total kinetic energy to fluctuate around $N k_B T$, insuring at the same time the correct (canonical) distribution of its fluctuations. A chain of 3 thermostats was employed with the first thermostat typical frequency equal to the highest phonon frequency of the lattice, $\omega_M = \{a^2 D + 2K(R_0(1 - \cos\theta)/\ell_0)^2]/m\}^{1/2}$. The integration of the corresponding equations of motion was again performed with a fourth-order Runge-Kutta scheme with typical time step of 0.01 t.u., and thermalization is achieved by a long-enough transient. Changes in temperature were performed in a sequential way upon heating the chain with a temperature ramp and relaxing afterward.

As discussed in Sec. IV, strictly speaking the transition is smooth. However the temperature range of the crossover region to a smooth behavior is so small (less than $\Delta T = 0.001$ K for a stacking parameter $b = 0.5$ Å^{-1}) that the numerical experiments, as well as actual denaturation experiments on DNA, show all the character of a first order transition. Therefore in this section we shall use the language of first order transitions which is the appropriate language to discuss the results.

Measured caloric curves showing the temperature (in energy units) as a function of the energy per degree of freedom, $k_B T(e)$, for a chain of $N = 128$ base pairs are reported in Fig. 8. They distinctly show a flat part at $k_B T = 0.2012D$ corre-
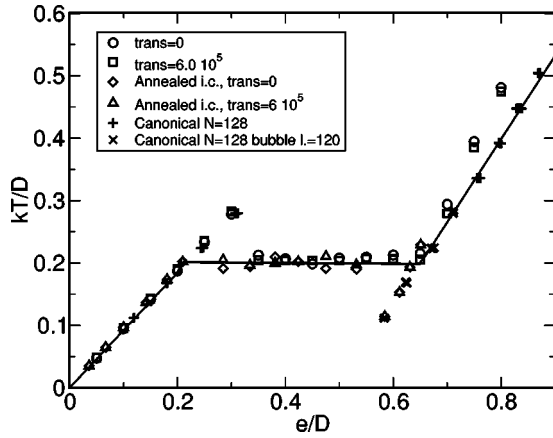
FIG. 8. Result of microcanonical simulations (open symbols): kinetic temperature as a function of the energy per degree of freedom for a molecule of $N = 128$ base pairs. To show the convergence of averages, data for two transient durations are reported. Pluses and crosses respectively refer to canonical simulations with closed initial conditions and with the initial insertion of an artificial bubble of length 120 base pairs (transient 10^5 time units). Solid line is the transfer integral result (see text for details).

sponding to the temperature $T_D = 350$ K that has been found to be the denaturation transition by the transfer integral calculation. In analogy with a liquid-gas transition, the flat region occurring between $e_B = 0.20D$ and $e_D = 0.64D$ is thus identified as the curve of coexistence between the closed and the denatured phases. The slope of the two branches, $k_B T/e$ should be equal to $2/c_v$ (the factor 2 appears because e, energy per degree of freedom is $\frac{1}{2}$ of the energy per unit cell). The figure shows that this is in good agreement with the values given by the TI calculation, i.e., $c_v \simeq 2.2$ below T_D and 1.5 above T_D. We have also compared the melting entropy per particle, $\Delta s = -\Delta(\partial f/\partial T)$, as obtained from the transfer integral calculation Δs_{th}, with that obtained from the microcanonical simulations Δs_{num} for the finite chain, i.e., the ratio $2(e_D - e_B)/T_D$:

$$\Delta s_{\text{num}} = 3.70 \times 10^{-4} \ \text{eV/K}, \quad \Delta s_{\text{th}} = 3.80 \times 10^{-4} \ \text{eV/K}. \tag{13}$$

The two quantities are in very good agreement.

In addition, the transition markedly displays a signature of *metastability and hysteretic effects*. Indeed, the B-DNA branch extends well above T_D (up to about 500 K). Marked hysteretic effect upon heating are also observed for the thermostated chain (crosses in Fig. 8). Either in microcanonical and canonical simulations, the system appears to be spontaneously "trapped" into this metastable state for low enough energies (or temperatures) over the transition one. Direct inspection of the system configuration reveals that the chain is completely closed and we can refer to it as an overheated state.

An undercooled branch exists as well below the denaturation temperature. To detect it in the microcanonical scheme, we employed the following procedure. The initial condition, in the B phase, is evolved for a certain time after which the chain is "annealed" by multiplying all velocities by an as-

signed factor smaller than 1 (we set it equal to 0.8). The averages are thus computed after a further transient (see again Fig. 8). Similar results can be obtained for the thermostated chain by artificially imposing on standard initial conditions the presence of a denatured bubble of given length ℓ in the middle of the chain at temperature $T > T_D$. We will give more details on this procedure at the end of this section.

Canonical and microcanonical results are therefore consistent, apart from some deviations at high temperatures, for $T > T_D$, which can be expected because after denaturation the model becomes almost purely harmonic as the Morse potential linking the bases plays no role for base-pair distance r corresponding to the plateau of the potential, and the stacking contribution also tends to vanish. Therefore for $T > T_D$ a microcanonical equilibrium cannot be achieved, unless we force it by averaging over thermalized initial conditions (for instance obtained by a Monte Carlo procedure) or by a temporary switch to a canonical simulation during a run.

The results were checked to be robust with respect to the transient duration as well as to the rate at which temperature is changed through the ramp. Alternative thermalization schemes do not change the outcomes as well. For example, simulations where microcanonical runs are alternated to canonical ones, yield the same results (except at $T > T_D$ as mentioned above). In such a case the computed averages are microcanonical as the thermostated dynamics only serves as a way to change the system energy.

Obviously, a crucial issue is the dependence of the results on the chain size. We observed that upon increasing the chain length up to $N = 256$ or 512, the only difference with respect to the $N = 128$ case is a slower convergence of the averages in the high and intermediate energy region. Nonetheless, the coexistence line is practically reached within comparable simulation times. This is presumably influenced by the initial conditions and could be improved by a more sensible choice.

In order to precise the nature of the transition from a view point close to experiments, we measured the average fraction of open base pairs ρ. This is indeed a quantity which is measurable by UV absorption. As in previous studies [15,18,20], we consider a base pair to be open whenever the radial displacement r_n is larger than the inflection point of the Morse potential, i.e., when $r_n/R_0 > 8 \ln 2$, and we average the counting during the run. A simple reasoning shows that the order parameter ρ should obey a "lever rule" [41]

$$e = (1 - \rho)e_B + \rho e_D, \quad e_B < e < e_D, \tag{14}$$

thus implying that $\rho(e)$ increases linearly between 0 and 1 along the coexistence line. In a similar way, we expect that the average twist per base pair $\langle \theta_n \rangle = \langle \phi_N - \phi_1 \rangle/N = \theta(1 + \sigma)$ should decrease linearly from a value close to θ to 0. This is illustrated in Fig. 9. Notice once again the hysteretic effects.

From Fig. 8 it is clear that the microcanonical ensemble has the merit of allowing to investigate the dynamics of the chain in the coexistence region. For illustration, Fig. 10 shows a snapshot of the state of the chain for $e/D = 0.5$ where, from formula (14), we expect around 40% of the base pairs to be denatured. The fact that the chain opens at the
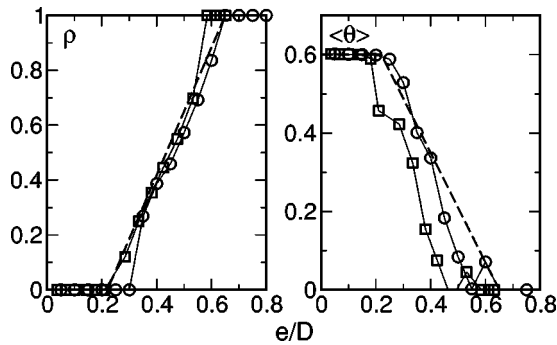
FIG. 9. Fraction of open base pairs ρ and average twist $\langle \theta_n \rangle$ from microcanonical simulations. The simulation parameters are the same as in Fig. 8. The circles were obtained with an initially closed chain while the squares refer to annealed initial conditions.

FIG. 11. Distributions of the lengths of the denatured regions at different times in the coexistence region $e=0.5D$. To improve the statistics, histograms were cumulated over a time window of around 10^3 time units.

sides is clearly caused by the free boundary conditions. Moreover, this figure can give a hint on why we observe a transition that has all the features of a true first order transition (coexistence of phases, metastability) although the transition is actually second order. From a theoretical point of view, the order is determined in the thermodynamic limit, i.e., for an infinite system. This correspond to the identification, in the transfer integral method, of the free energy with the lowest eigenvalue ϵ_0, Eq. (5). In numerical simulations, as well as in experiments, one is dealing with a finite system. When the thermodynamic transition is extremely sharp (as it is the case for the stacking parameter $b=0.5$ Å^{-1}), the inhomogeneity caused by the free ends is sufficient to lead to an apparent coexistence of phases, i.e., a first-order-like transition, presumably because the boundary effects induce a perturbation (in particular on the average local torque) which is sufficient to change the local transition temperature by the very small amount which separates the domain of closed DNA from the domain where the molecule denaturates. This is why the molecular dynamics simulations are useful to
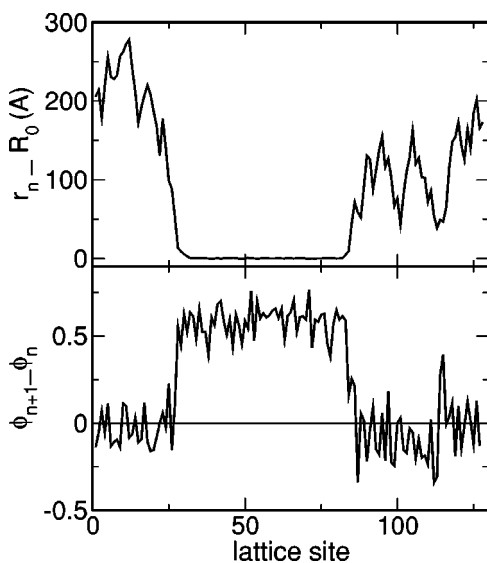

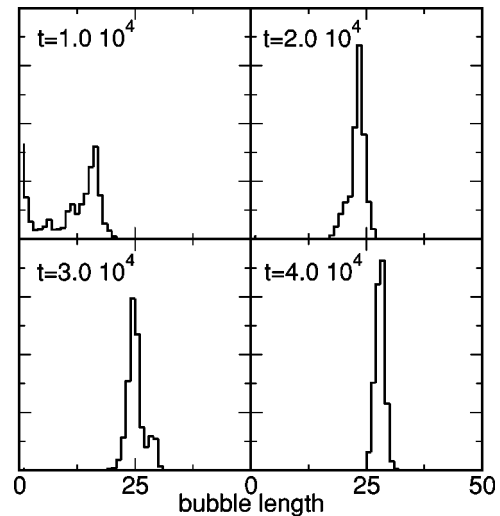FIG. 10. Snapshot of the chain of 128 bps in the coexistence region $e=0.5D$.

complete the transfer integral study, and to provide results that can be compared with experiments.

Another interesting aspect which can be studied through simulation is the dynamics of opening events. This allows to look for analogies with the classical nucleation mechanisms that drives relaxation from metastable states at ordinary first-order transitions [41]. Figure 11 reports the distribution of the length of denatured bubbles for subsequent times during the same run of Fig. 10. There is a clear tendency for smaller bubbles to close (or merge) until only a few large ones remain. A similar measure in the overheated metastable phase shows instead that the size of bubbles is pretty small and decrease systematically in time.

To further investigate this aspect, we performed simulations in the canonical ensemble, starting from a thermalized state at temperature T and artificially seeding a denatured bubble of given length ℓ in the middle of the chain. To accomplish this, given the geometry of the model, we set $\theta_n=0$ in the central region and impose a triangular profile for the r_ns designed in such a way that the resulting stress on the backbone springs is approximatively zero. The flanking regions are initially at equilibrium and free from any additional supercoiling.

In a first series of simulations we checked that for $T < T_D$ the B-DNA form is very robust with respect to such local perturbation: for instance, at $T=200$ or 300 K bubbles of length $\ell \leq 12$ base pairs on a chain 128 base-pair long tend to shrink and the system rapidly returns to its completely closed state. Very large bubbles ($\ell \sim 110$ base pairs) may tend to close as well, although on longer times. However, several cases are found where perturbations as large as $\ell = 120$ base pairs are able to drive the system into the metastable, undercooled, denatured state. These experiment allow the observation of the second metastable state in the canonical scheme: thus completing the correspondence with the microcanonical results (see again data shown in Fig. 8).

The situation is, as expected, the opposite in the over-

heated region $T_D < T \lesssim 600$ K. Here, the insertion of a short bubble suffices to destabilize the B-DNA form and let the system switch to its equilibrium state, i.e., the completely open chain. For instance, at $T = 400$ or 500 K a bubble of length $\ell > 8$ on a chain of 128 base pairs is generally enough. Approximated estimates seem to indicate that the minimal length of the bubble tend to decrease with temperature, as intuitively expected, but this behavior is not very systematic. Statistics over a very large number of events would be necessary to conclude quantitatively.

VI. DYNAMICAL STRUCTURE FACTORS

One of the motivations for considering mechanical models is the possibility to probe microscopic and collective motion in different phases. In this section, we focus on dynamical correlation functions that usually reflect different types of excitations. More precisely, we computed the radial structure factor

$$S_r(q,\omega) = \left\langle \left| \int \sum_n r_n e^{i(qn - \omega t)} dt \right|^2 \right\rangle \quad (15)$$

and the angular one $S_\psi(q,\omega)$ where $\psi_n = \phi_n - n\theta$ is the angular displacement from the equilibrium position. Brackets denote an average over an ensemble of independent molecular dynamics trajectories (typically hundreds). All the results reported in this section are obtained in the microcanonical ensemble.

Let us first consider the low temperature native phase. As shown in Fig. 12, the spectral analysis display, as expected, sharp lines at the frequencies of the two phonon branches $\omega_\pm(q)$ that can be computed at $T = 0$ in the harmonic approximation [27] (see the vertical lines in Fig. 12). Acoustic vibrations in the angular variables are only weakly coupled to the radial (optical) ones. Interesting enough, the radial spectra also displays a large peak at a frequency lying in the phonon gap and independent on the wave number [i.e., the large peak at $\omega \simeq 0.7$ in Fig. 12(a)]. Its origin can be traced back to the excitation of a localized surface mode. This is confirmed by direct inspection of the chain configuration. Actually, the mode is found to slowly decay in time due to nonlinear interaction leading to a systematic decrease of its spectral component.

Upon increasing the energy, the optical branch gradually shifts towards lower values of the frequency (softening) and higher-harmonics appear. Furthermore, the resonances in both the radial and angular peaks are substantially broadened due to increasing anharmonicity that enhances the effective damping. More importantly, a large low-frequency component, a *central peak*, arises in the radial structure function. The temperature dependence of $S_r(q,\omega)$ across the denaturation transition is illustrated in Fig. 13. The three different energies correspond to $T = 300$, 357, and 535 K. The latter value is well into the metastable overheated region. For fixed q, the position of the central peak is unchanged upon increasing temperature but its width broadens. Furthermore, the ω^{-2} behavior at low frequencies (see the inset of Fig. 13) suggests a Lorentzian line shape. The origin of this central
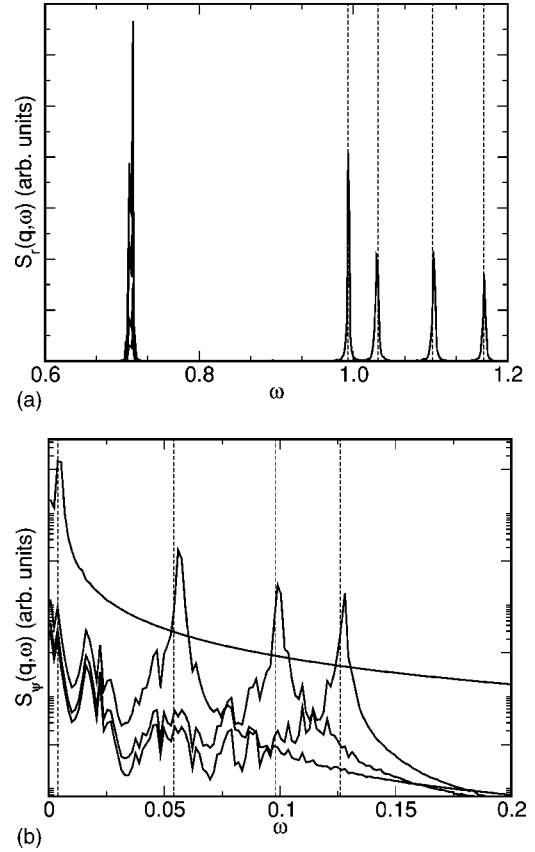

(a)

(b)

FIG. 12. Structure factors $S_r(q,\omega)$ (a) and $S_\psi(q,\omega)$ (b) for $N = 256$ at very low energy, $e = 0.01D$ (corresponding to $T = 18$ K). The different curves correspond to wave numbers $q = 2.5676$, 1.66896, 0.88356, and 0.09812 (right to left).

peak, also found in the simpler PB model, and its properties are still unclear although it is tempting to assign it to the slow dynamics of the bubble boundaries.

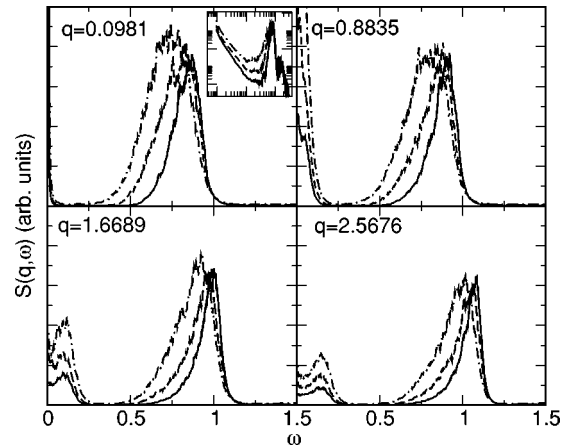An even more sizable central component appears when closed and open form coexist (see Fig. 14). This is accom-

FIG. 13. Radial structure factors $S_r(q,\omega)$ for $N = 256$ and different energies $e = 0.17D$, $0.20D$, and $0.30D$ (solid, dashed, and dot-dashed lines, respectively). To reduce fluctuations, a smoothing of the data has been performed by averaging over 10 consecutive channels.
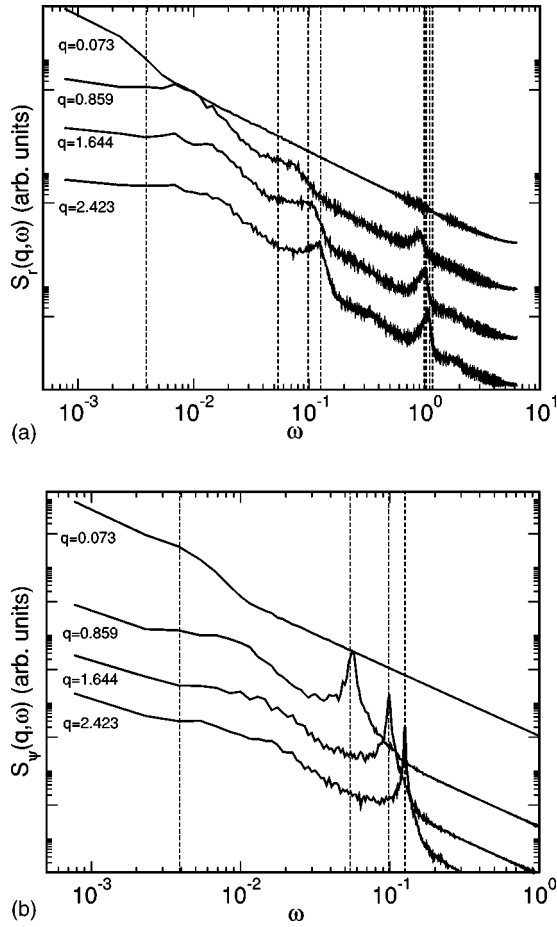
FIG. 14. Structure factors $S_r(q,\omega)$ and $S_\psi(q,\omega)$ for $N=256$ in the coexistence region $e=0.50D$. Vertical lines are the phonon frequencies (one from the acoustic and one from the optical branch for each q value) calculated at $T=0$. Graphs have been arbitrarily shifted for clarity.

panied by a stronger coupling between angular and radial degrees of freedom, as manifested by the peaks at acoustic frequencies in S_r. The birth of large low-frequency components bears strong resemblance with heterophase fluctuations observed in other lattice models with (pseudo) first-order transition characterized by large entropy barriers [36–38]. In other words, the motion of the interface between the two phases should be responsible for the slow dynamics.

To close this section, it is worth mentioning that a related analysis of collective modes for the helicoidal model has been recently reported [42]. The analytical calculations were performed at room temperature and are based on the instantaneous normal modes. At variance with our simulations, this approach describe the short-time dynamics (on a time scale of picoseconds) and a direct comparison is therefore not straightforward.

VII. CONCLUSIONS AND DISCUSSION

The study of a simplified model of DNA has proved to be extremely fruitful to unveil the basic features of the melting transition at the single-molecule level. From the theoretical

point of view, dealing with a one-dimensional model (with two degrees of freedom per base pair) turned out to be particularly convenient as it allows an exact evaluation of the partition function. Indeed, the angular variables can be eliminated by Fourier transform, yielding a more tractable one-variable transfer integral problem. The latter cannot be solved analytically but the numerical and approximate results presented above provide a complete insight on the nature of the transition. In particular, the finite-size scaling analysis of the transfer integral turned out to be essential to take into account the finiteness of the integration range. Such an analysis strongly suggests that the underlying transition is continuous, of the Kosterlitz-Thouless type. This behavior can be related to the existence of an effective attractive force which is *directly connected to the helicoidal geometry* because it appears when the angular degree of freedom is integrated out. Qualitatively it can be understood as coming from the difficulty to disentangle the two helices. On the other hand, for physically relevant values of the parameters, the temperature range over which the continuous aspect of the transition can be detected may become extremely narrow (less than $\Delta T = 0.001$ K). For all practical purposes the transition appears to be perfectly sharp, and bears the hallmarks of a first order transition, in agreement with experiments. In our view, this result is remarkable and attracts attention on how numerical or experimental observations on finite systems and with a limited resolution may dramatically differ from theoretical expectations.

Molecular dynamics simulations confirm this apparent first-order character. They show hysteresis and metastability as well as a coexistence region between an open and a closed "phase" and, by varying the energy density in the critical region, a gradual change of the volume fraction occupied by the two which is reminiscent of, say, the liquid-gas transitions.

In addition to the very sharp transition found by the theoretical analysis, the finite-size effects certainly play a major role in the above phenomenology. The helicoidal model is more sensitive to these finite size effects than the "flat" PB model because the free ends allow a release of the torsional energy which appears when a segment of the chain opens. One can understand the crucial role of boundary effects if one considers that a finite closed loop of helicoidal DNA cannot denaturate at all because the two strands are entangled.

The dynamics of the transition, as probed by the calculation of the radial and angular structure factors, shows some prominent features such as the existence of a central peak that is presumably due to the slow motion of the denaturation bubbles. Moreover, the coupling between opening and twist introduces some additional spectral features that would deserve further investigations.

Another point that should be reconsidered is the nucleation of denaturation bubbles. The phenomenology described at the end of Sec. V is, at least qualitatively, very much reminiscent of the nucleation mechanisms that drives relaxation from metastable states at ordinary first-order transitions [41]. For instance, simulation in the overheated state suggests the existence of a "critical size" of the denaturation

loops, above which they become unstable. Hence, metastability stems from the fact that small enough bubbles close relatively fast. Nevertheless, there are important differences that one should keep in mind. Indeed, in classical nucleation theory the key role is played by the surface tension term (proportional to the square of the droplet's radius), whereby in our one-dimensional case the bubble "surface" is independent of its length. The correspondence with the usual theory is probably due to the torsional energy, associated to the opening, which grows with the bubble size. This suggests that a "one-dimensional nucleation theory" could be developed for helicoidal DNA.

The present study has focused on a DNA model that describes the molecule at the scale of the base pair. We think that it is relevant because it is the scale of the genetic code at which phenomena related to biological functions occur. The helicoidal geometry itself is at this scale (or more precisely at the scale of a few tens of base pairs). On the other hand, there are other phenomena that enter in the statistics of DNA melting, and they are related to the behavior of the molecule at a much larger scale, on which the strands are regarded as flexible strings. Recent studies have shown that the entropy of the loops also contributes to lead to a first order transition, provided that self-avoiding aspects between segments of the loop and between open regions and closed domains are properly taken into account [11]. Our approach is complementary to these studies and shows that the observed sharp melting transition of DNA may have multiple origins.

APPENDIX: RESULTS OBTAINED VIA GRADIENT EXPANSION

1. An approximate TI kernel

In the absence of an external torque, the nontrivial part of the partition function of the model is given by

$$Z_P = \int \prod_{n=1}^{N} \{dr_n[r_n r_{n-1}]^{1/2} d\theta_n\} e^{-V(\{r_i, \theta_i\})/k_B T}, \quad (A1)$$

where the potential energy consists of the three last terms in Eq. (1), and the relative angle coordinate enters only via the second term. Introducing sum and difference coordinates $\bar{r}_n = (r_n + r_{n-1})/2$, $\delta_n = r_n - r_{n-1}$, it is possible to write the integral over θ_n as

$$\int_0^\pi d\theta_n e^{-K(l_{n,n-1} - \ell_0)^2/k_B T} \equiv \Phi_0(\bar{r}_n) e^{\Omega(\delta_n^2, \bar{r}_n)}. \quad (A2)$$
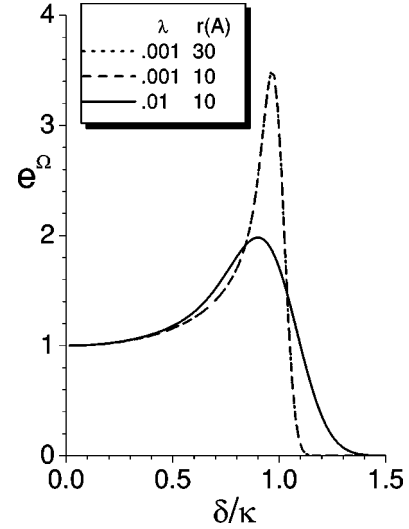

FIG. 15. $\exp(\Omega)$ as a function of δ/κ for two different values of the dimensionless ratio λ; the r dependence is not visible for $\lambda = 0.001$.

For the parameter values given in Table I, and $T = 480$ K, the dimensionless ratio $\lambda = k_B T / K R_0^2$ is equal to 0.01; this allows us to use the leading-order low-temperature asymptotic expansion

$$\Phi_0(\bar{r}) \sim \sqrt{\frac{\pi k_B T}{K}} \frac{L_0}{\kappa \bar{r}} \left(1 - \frac{\kappa^2}{4\bar{r}^2}\right)^{-1/2}, \quad (A3)$$

where $\kappa = 2R_0 \sin(\theta/2) = 5.98$ Å, over the whole temperature range of interest. Note that due to the repulsive core of the Morse potential, the inequality

$$r \gg \kappa/2 \quad (A4)$$

always holds. Furthermore, numerical evaluation reveals that the function Ω is (i) almost independent of $\bar{r}$, and (ii) weakly dependent on temperature (cf. Fig. 15). In the following we will use the temperature-independent approximation

$$e^{\Omega(\delta^2)} \approx e^{-(\delta/\kappa)^2}, \quad (A5)$$

which misses the weak peak near $\delta = \kappa$, but reproduces correctly the second moment, which is central to what follows. Within the approximations (A3), (A4), the partition function is dominated, in the thermodynamic limit, by the largest eigenvalue of the one-dimensional TI equation

$$\int_0^\infty dr' T(r, r') \psi_\nu(r') = \Lambda_\nu \psi_\nu(r) \quad (A6)$$

with

$$T(r, r') \approx \sqrt{\frac{\pi k_B T}{K}} \frac{L_0}{\kappa} \left(1 + \frac{\kappa^2}{8\bar{r}^2}\right)\left(1 - \frac{\delta^2}{8\bar{r}^2}\right)$$
$$\times e^{\Omega(\delta^2)} e^{-V_M(r)/k_B T} e^{-V_S(\bar{r}, \delta^2)/k_B T}, \quad (A7)$$

where $V_M(r) = D(1 - \exp[-a(r-R_0)])^2$ and $V_S = S\delta^2$ $\times \exp[-2b(\bar{r}-R_0)]$.

The form of Ω [cf. Fig. 15 and/or Eq. (A5)] establishes that, in addition to the ranges $1/a$, $1/2b$ of the Morse and stacking interactions, respectively, there is a third, much larger, characteristic length in the problem, κ. Depending on the strength of the various parameters, it may be possible to further simplify the general one-dimensional TI problem and elucidate the ensuing critical behavior. Two distinct cases will be considered below.

2. Strong stacking interaction: transformation to an ODE

A gradient expansion of Eq. (A6) involves (i) introducing

$$\psi_\nu(r+\delta) \approx \psi_\nu(r) + \psi'_\nu(r)\delta + \frac{1}{2}\psi''_\nu(r)\delta^2, \quad \text{(A8)}$$

(ii) changing the variable of integration from r' ($= r + \delta$) to δ, and (iii) performing the Gaussian integrals over δ. Noting that (a) the combined effect of the stacking interaction and the Gaussian approximation (A5) can be described in terms of the quantity

$$\frac{S}{k_BT}\mu^2(r) \equiv \frac{S}{k_BT}e^{-2b(r-R_0)} + \frac{1}{\kappa^2} \quad \text{(A9)}$$

(note that $S\mu^2$ can be interpreted as an effective nearest neighbor harmonic spring constant) and that (b) $\bar{r} \approx r$ to second order in δ everywhere in Eq. (A7), one obtains

$$\left(1 - \frac{k_BT}{16S\mu^2r^2}\right)\psi_\nu + \frac{k_BT}{4S\mu^2}\psi''_\nu = e^{-\beta(\epsilon_\nu - U_1)}\psi_\nu, \quad \text{(A10)}$$

where $U_1(r) = V_M(r) + V_L(r) + V_B(r)$ and $\Lambda_\nu = (\pi k_BT/\sqrt{KS})\ell_0/\kappa e^{-\beta\epsilon_\nu}$; here, $V_L(r) = -k_BT(\kappa/r)^2/8$ is a long-range attraction which comes from exponentiating the term in the first parentheses of Eq. (A7), and $V_B(r) = k_BT\ln[\mu(r)/\mu(\infty)]$ is a thermally generated barrier analogous to the one described in [8] in the context of the one-dimensional DNA model with stacking. Expanding the exponential in the right-hand side (RHS) of Eq. (A10) and rearranging terms, one obtains

$$-\frac{(k_BT)^2}{4S\mu^2}\psi''_\nu + (V_M + V_B + V_L^*)\psi_\nu = \epsilon_\nu\psi_\nu, \quad \text{(A11)}$$

where

$$V_L^*(r) = V_L(r)\left[1 - \frac{1}{2}\left(\frac{\mu(\infty)}{\mu(r)}\right)^2\right] \quad \text{(A12)}$$

is attractive everywhere.

Equation (A11) is a key result. It can be trivially cast in standard Sturm-Liouville form with a density function proportional to μ^2; the r dependence of μ is crucial for obtaining quantitatively sensible results; the simultaneous presence of three terms in the potential energy prevents us from solving Eq. (A11) exactly. A numerical solution [43] for the parameter values of Table I reveals a behavior very similar to
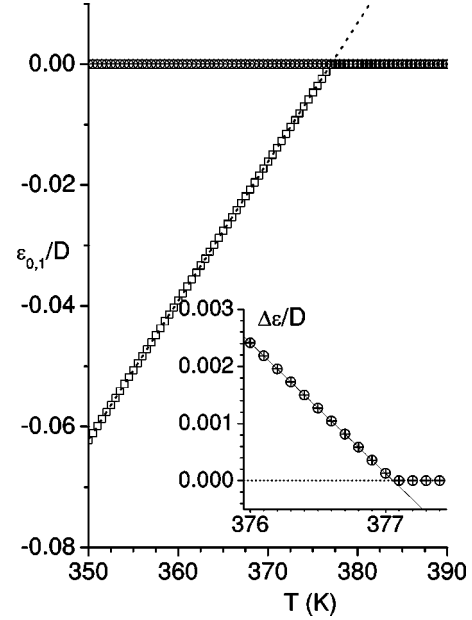

FIG. 16. The numerically determined two lowest eigenvalues of Eq. (A11), expressed in units of D. The onset shows details of the gap in the region of the transition; no signs of rounding are apparent at a sampling of $\Delta T = 0.1$ K.

the full TI solution of Sec. IV. According to Fig.16, the two lowest eigenvalues exhibit an almost perfect intersection at a temperature sampling $\Delta T = 0.1$ K. In addition, the differential equation turns out to be an excellent approximation to the original TI. Thus, the estimated $T_D = 370$ K is only a few percent higher than the value obtained within the TI; other critical thermodynamic quantities of interest demonstrate comparable, or better agreement, e.g., the transition enthalpy $\Delta H = T_D\Delta S = 0.129$ eV (cf. 0.133 eV from TI), or the jump in the specific heat, $0.8k_B$ (cf. $0.7k_B$ from TI). The apparent first-order transition has its origin in the fact that the thermally generated barrier has a substantially longer range than the Morse potential. The analysis of Sec. IV suggests that crossover to a continuous transition eventually occurs; however, for the values of the parameters relevant to DNA denaturation, observing this exponential crossover would require a temperature resolution of better than 1 mK. This estimate can be made by studying crossover phenomena with exactly solvable "toy models" [32] of the denaturation transition of the linear PB variety, where the zero stacking limit is known to yield a second-order "underlying" transition. In the case of Eq. (A11), the presence of an attractive inverse square interaction raises the possibility of more complex behavior, i.e., confinement at all temperatures or crossover to another transition at much higher temperatures. This is discussed below.

3. The $S = 0$ case

In the limit $S \to 0$, the decay of the kernel (A7) is governed by Eq. (A5). This reduces Eq. (A11) to

$$-k_BT\frac{\kappa^2}{4}\psi''_\nu + (V_M + V_L^*)\psi_\nu = \epsilon_\nu\psi_\nu, \quad \text{(A13)}$$

where

$$V_L^*(r) = -k_B T \frac{\kappa^2}{16r^2}. \tag{A14}$$

In the absence of stacking, the system is subject to the Morse potential and the long-range attraction (A14); the point to note is that the attractive force is linearly dependent on the temperature, just as the coefficient of the 2nd derivative in Eq. (A13); consequently, if $D=0$, the system will either have a bound state or not, according to the value of the coefficient in the denominator of Eq. (A14). The value 16 is marginal; if the interaction had been stronger, one would have confinement at all temperatures; the Morse potential, being of short range, could not change that; in other words, one would obtain a near-transition at a temperature controlled by the Morse potential, but then the long-range attrac-

tion would prevent dissociation at all temperatures. We have verified this by numerically solving Eq. (A13). For weaker attractions (value of the coefficient 16 or higher in these units), numerical work suggests that the transition becomes higher than second order; however, numerical accuracy is not sufficient to determine the detailed behavior. It is possible to guess what happens by substituting the Morse potential by a narrow well, i.e., the total potential in Eq. (A13) being equal to $-D$ for $R_0 < r < R_0 + 1/a$ and equal to Eq. (A14) for larger r; this case is exactly solvable and shows that although the shift in the value of the critical point is less than 1%, the nature of the transition is radically transformed: the vanishing of the lowest eigenvalue is now of the Kosterlitz-Thouless type

$$\epsilon_0 \propto -e^{-\text{const}/(T_D - T)}. \tag{A15}$$

[1] L. V. Yakushevich, *Nonlinear Physics of DNA* (Wiley, Chichester, 1998).

[2] T. Strick *et al.*, Physica A **263**, 392 (2000).

[3] U. Bockelmann, B. Essevaz-Roulet, and F. Heslot, Phys. Rev. E **58**, 2386 (1998).

[4] R.M. Wartell and A.S. Benight, Phys. Rep. **126**, 67 (1985).

[5] B.H. Zimm, J. Chem. Phys. **33**, 1349 (1960).

[6] M. Ya Azbel, Phys. Rev. Lett. **31**, 589 (1973).

[7] M. Ya Azbel, J. Phys. A **12**, L29 (1979).

[8] N. Theodorakopoulos, T. Dauxois, and M. Peyrard, Phys. Rev. Lett. **85**, 6 (2000).

[9] T. Dauxois, N. Theodorakopoulos, and M. Peyrard, J. Stat. Phys. **107**, 869 (2002).

[10] M.S. Causo, B. Coluzzi, and P. Grassberger, Phys. Rev. E **62**, 3958 (2000).

[11] Y. Kafri, D. Mukamel, and L. Peliti, Phys. Rev. Lett. **85**, 4988 (2000).

[12] E. Carlon, E. Orlandini, and A.L. Stella, Phys. Rev. Lett. **88**, 198101 (2002).

[13] M. Peyrard and A.R. Bishop, Phys. Rev. Lett. **62**, 2755 (1989).

[14] T. Dauxois, M. Peyrard, and A.R. Bishop, Phys. Rev. E **47**, 684 (1993).

[15] T. Dauxois and M. Peyrard, Phys. Rev. E **51**, 4027 (1995).

[16] A. Campa and A. Giansanti, Phys. Rev. E **58**, 3585 (1998).

[17] D. Cule and T. Hwa, Phys. Rev. Lett. **79**, 2375 (1997).

[18] M. Barbi, S. Cocco, M. Peyrard, and S. Ruffo, J. Biol. Phys. **24**, 97 (1999).

[19] M. Barbi, S. Cocco, and M. Peyrard, Phys. Lett. A **253**, 358 (1999).

[20] S. Cocco and R. Monasson, Phys. Rev. Lett. **83**, 5178 (1999).

[21] S. Cocco, M. Barbi, and M. Peyrard, Phys. Lett. A **253**, 161 (1999).

[22] A. Campa, Phys. Rev. E **63**, 021901 (2001).

[23] G. Gaeta, Phys. Lett. A **168**, 383 (1992).

[24] H. Grimm and A. Rupprecht, Physica B **234-236**, 183 (1999).

[25] H. Urabe *et al.*, J. Chem. Phys. **95**, 5519 (1991).

[26] Following Ref. [20] we also make the further simplification to neglect the curvature terms originally introduced in Ref. [18]. This also eases the determination of the model parameters on the basis of the experimental data.

[27] M. Barbi, Ph.D. thesis, University of Florence, 1998.

[28] T. Strick *et al.*, Science **271**, 1835 (1996).

[29] S. Cocco, Ph.D. thesis, University of Rome–La Sapienza and ENS-Lyon, 2000.

[30] I. Abramowitz and A. Stegun, *Handbook of Mathematical Functions* (Dover, New York, 1965).

[31] R. Courant and D. Hilbert, *Methods of Mathematical Physics* (Wiley, New York, 1989).

[32] N. Theodorakopoulos (unpublished).

[33] N. Theodorakopoulos, in *Proceedings of the Third Conference "Localization and Energy Transfer in Nonlinear Systems," San Lorenzo de El Escorial, Spain*, edited by L. Vàzques, R.S. MacKay, and M.P. Zorzano (World Scientific, Singapore, 2002), p. 130; e-print cond-mat/0210188.

[34] M.E. Fisher and M.N. Barber, Phys. Rev. Lett. **28**, 1516 (1972).

[35] N. Theodorakopoulos, Phys. Rev. E **68**, 026109 (2003).

[36] R.J. Gooding and J.R. Morris, Phys. Rev. E **47**, 2934 (1993).

[37] W.C. Kerr, A.M. Hawthorne, R.J. Gooding, A.R. Bishop, and J.A. Krumhansl, Phys. Rev. B **45**, 7036 (1992).

[38] J.R. Morris, Ph.D. thesis, Cornell University, 1993.

[39] For constant-energy simulation, it would be more proper to use a symplectic algorithm. However, implementation would be awkward for nonstandard Lagrangians like ours as it would require implicit schemes. Therefore we preferred to avoid this technical difficulty.

[40] G.J. Martyna, M.L. Klein, and M. Tuckerman, J. Chem. Phys. **97**, 2635 (1992).

[41] H.B. Callen, *Thermodynamics and an Introduction to Thermostatics* (Wiley, New York, 1985).

[42] S. Cocco and R. Monasson, J. Chem. Phys. **112**, 10017 (2000).

[43] We have used the IMSL subroutine DSLEIG in the semi-infinite interval 9.7 Å $< r < \infty$.